Monte Carlo Simulations for Clutter Statistics in Minefields: AP-Mine-Like-Target Buried Near a Dielectric Object Beneath 2-D Random Rough Ground Surfaces

Magda El-Shenawee, *Member, IEEE,* and Carey M. Rappaport, *Senior Member, IEEE*

***Abstract*—A rigorous three-dimensional (3-D) electromagnetic model is developed to analyze the scattering from anti-personnel (AP) nonmetallic mine-like target when it is buried near a clutter object under two-dimensional (2-D) random rough surfaces. The steepest descent fast multipole method (SDFMM) is implemented to solve for the unknown electric and magnetic surface currents on the ground surface, on the target and on the clutter object. A comprehensive numerical investigation of two clutter sources; the ground roughness and the nearby benign object, is presented based on using more than 800 random rough surface realizations which could not be achieved without using fast algorithms such as the SDFMM. The statistics of the scattered near-electric fields are computed using the Monte Carlo simulations for both polarizations. For the parameters used here, the results show that the average and the standard deviation of the target signature represent 5–7% and 3–3.5% of the total scattered signal, respectively, while they represent 16–20% and 7–12% of the signal for the clutter object, respectively. This study indicates the high possibility of a false alarm during the detection process when the target is located nearby a realistic object such as a piece of a tree root.**

***Index Terms*—Clutter statistics, Monte Carlo simulations, multiple buried objects, rough surface scattering, SDFMM, subsurface sensing.**

I. Introduction

ELECTROMAGNETIC sensing of targets buried in soil with two-dimensional random rough surface necessitates the investigation of clutter sources that may cause false alarms in the detection process. In real minefields, there are a variety of clutters that can easily obscure the signal of the target such as: the roughness of the ground, nearby benign objects (e.g., tree roots, rocks, etc.), spots of concentrated inhomogeneity in the soil, etc. Detecting small anti-personnel nonmetallic mines is very difficult as it is, but proximity of clutter objects obscures target detection considerably.

The statistics of the scattered waves from the random rough ground were previously investigated in the literature either analytically, [1]–[4], or computationally using the Monte Carlo simulations, [5]–[10]. The challenging part of conducting the Monte Carlo simulations is to run a 3-D computer code hundreds of times when the rough ground has large electrical size and contains multiple penetrable objects buried under the interface. In [1]–[4], integral expressions were developed to calculate the incoherent radar cross section (RCS) of the rough ground (no buried objects). These integrations were basically obtained by considering the ground heights and slopes as random variables producing analytic closed forms in some cases (e.g., at high frequency). On the other hand, conducting the Monte Carlo numerical simulations were used to obtain the incoherent RCS of the rough surface without buried objects in [5]–[8], to obtain the RCS and/or the angular correlation function of a PEC sphere buried under the rough interface [9] and to obtain the statistical average of the scattered near-fields when a penetrable object was buried under the interface in [10].

In our previous work [10] and [11], we implemented the steepest descent fast multipole method (SDFMM) [6], [12] to investigate the effect of the ground roughness on the signature of a single target buried under the ground. The $O(N)$ computational complexity of the SDFMM accelerated the calculations of the unknown surface currents on the shallow mine-like object buried beneath a moderately random rough ground especially in conducting the Monte Carlo simulations. Similarly, to study the influence of the ground roughness (with no buried targets) on the scattered signals for different minefields, the SDFMM was used to run the Monte Carlo simulations from Puerto-Rican and Bosnian soils [13].

To the best of our knowledge, no work is published for investigating the statistics of multiple objects buried under the 2-D random rough ground, which is the objective of this paper. In [14], rigorous generalized electromagnetic formulations were developed for scattering from multiple objects buried under the rough ground, where the SDFMM was implemented to speed up the computations. A parametric investigation is conducted in [14] to study the effect on the scattered signature due to the objects proximity, ground roughness, object's material, shape, location, etc. A variety of object shapes were studied in [14], e.g., one object is spheroid and the second object is ellipsoid, spheroid, disk, or horizontal cylinder.

In this paper, we are using the Monte Carlo simulations to conduct a statistical study of mine-like dielectric target's signature versus the clutter signature due to both the ground roughness and a benign object as shown in Fig. 1. Even though, we

Manuscript received November 14, 2001; revised April 22, 2002. This work was supported by the Northeastern University's Demining MURI Grant DAA 0-55-97-0013 and the ERC Program of the NSF Award EEC-9986821.

M. El-Shenawee is with the Department of Electrical Engineering, University of Arkansas, Fayetteville, AK 72701 USA (e-mail: magda@uark.edu).

C. Rappaport is with the Department of Electrical and Computer Engineering, Northeastern University, Boston, MA 02115 USA (e-mail: rappaport@neu.edu).

Publisher Item Identifier 10.1109/TGRS.2002.800275.

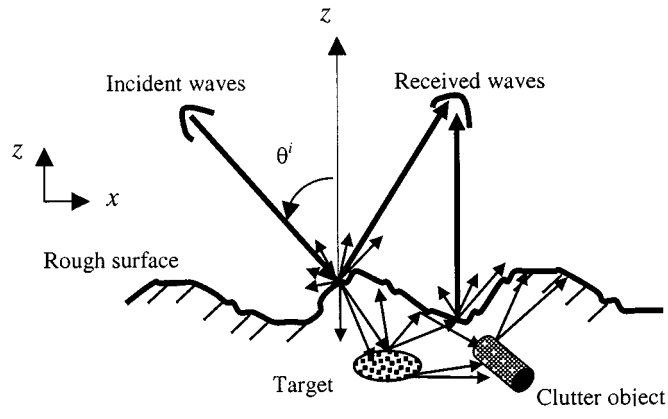

Fig. 1. Cross section of a target buried near a clutter object beneath the rough ground surface.

are emphasizing here only on these two types of clutter, however, there are additional types of clutter that may significantly affect the target signature such as the soil inhomogeneities and the multilayered nature of the ground, which are not accounted for in this work. According to the United States Department of Defense data (U.S. DoD), European agencies and others, it is a fact that there are hundreds of different types, shapes and manufacturers of the AP-plastic mines. This is one of the reasons that these mines are difficult to detect. In this work, we are not modeling a specific type of these mines but instead modeling a plastic-mine-like target that has a shape very close to an oblate spheroid. Several examples of spheroid-shape types can be obtained from the U.S. DoD CD-ROM Humanitarian Demining Equipment database.In Section II the formulations of the electromagnetic model developed in [14] are summarized, numerical results are shown in Section III and conclusions are drawn in Section IV.

II. Problem Formulations

The rigorous electromagnetic model developed in [14] is employed in this work to conduct the Monte Carlo simulations for two objects buried under the 2-D random rough ground as shown in Fig. 1. The inhomogeneous scatterer is composed of four different regions; air R_1, ground R_2, target R_3 and clutter object R_4 where the relative permittivity and permeability are (ε_1, μ_1), (ε_2, μ_2), (ε_3, μ_3) and (ε_4, μ_4), respectively, as shown in Fig. 2(a). The unknown equivalent electric and magnetic surface currents are $(\bar{J}_1, \bar{M}_1)$ on S_1, $(\bar{J}_3, \bar{M}_3)$ on S_2 and $(\bar{J}_5, \bar{M}_5)$ on S_3. The final set of surface integral equations on S_1, S_2 and S_3 in Fig. 2(a) are given by [14] (1a)–(1f), shown at the bottom of the page, in which the intrinsic impedance is $\eta_i = \sqrt{\mu_i/\varepsilon_i}$ in region R_i with $i = 1, 2, \ldots 4$ and L_j and K_j, $j = 1, 2, \ldots 6$ are the integro-differential operators given in Appendix A. The tangential component of the incident electric and magnetic fields on the rough surface S_1 are given by $\bar{E}^{inc}(\bar{r})\big|_{\text{tang}}$ and $\bar{H}^{inc}(\bar{r})\big|_{\text{tang}}$. The surfaces S_1, S_2 and S_3 are discretized into triangular patches where the unknown equivalent electric and magnetic currents in (1) are approximated by using the Rao, Wilton, and Glisson (RWG) vector basis functions $\bar{j}(\bar{r})$ [15], [16] as

$$\begin{aligned} \bar{J}_i(\bar{r}) &= \sum_{n=1}^{N_k} I_{in}\bar{j}_{kn}(\bar{r}) \\ \bar{M}_i(\bar{r}) &= \eta_1 \sum_{n=1}^{N_k} I_{(i+1)n}\bar{j}_{kn}(\bar{r}), \bar{r} \in S_k, \\ &\text{for } i = 1, 3, \text{ and } 5 \end{aligned} \tag{2}$$

and $k = (i+1)/2$. Upon substituting (2) in (1) and testing using the same vector basis functions, the linear system of equations is obtained [14]

$$\bar{\bar{Z}}\bar{I} = \bar{V} \Rightarrow \begin{pmatrix} \bar{Z}_{11} & \bar{Z}_{12} & \bar{Z}_{13} \\ \bar{Z}_{21} & \bar{Z}_{22} & \bar{Z}_{23} \\ \bar{Z}_{31} & \bar{Z}_{32} & \bar{Z}_{33} \end{pmatrix} \begin{pmatrix} I^1 \\ I^2 \\ I^3 \end{pmatrix} = \begin{pmatrix} \bar{V}_1 \\ 0 \\ 0 \end{pmatrix}. \tag{3}$$

The total matrix $\bar{\bar{Z}}$ has order of $2(N_1+N_2+N_3) \times 2(N_1+N_2+N_3)$, where the number of unknowns on the ground, on the target and on the clutter object are $2N_1$, $2N_2$ and $2N_3$, respectively. It is necessary to emphasize that this rigorous electromagnetic model considers all scattering and

$$\bar{E}^{inc}(\bar{r})\big|_{\text{tang}} = \left[(L_1+L_2)\bar{J}_1 - (K_1+K_2)\bar{M}_1 - L_3\bar{J}_3 + K_3\bar{M}_3 - L_4\bar{J}_5 + K_4\bar{M}_5\right]_{\text{tang}}, \bar{r} \in S_1 \tag{1a}$$

$$\bar{H}^{inc}(\bar{r})\big|_{\text{tang}} = \left[(K_1+K_2)\bar{J}_1 + \left(\frac{L_1}{\eta_1^2} + \frac{L_2}{\eta_2^2}\right)\bar{M}_1 - K_3\bar{J}_3 - \frac{L_3}{\eta_2^2}\bar{M}_3 - K_4\bar{J}_5 - \frac{L_4}{\eta_2^2}\bar{M}_5\right]_{\text{tang}}, \bar{r} \in S_1 \tag{1b}$$

$$0 = \left[-L_2\bar{J}_1 + K_2\bar{M}_1 + (L_3+L_5)\bar{J}_3 - (K_3+K_5)\bar{M}_3 + L_4\bar{J}_5 - K_4\bar{M}_5\right]_{\text{tang}}, \bar{r} \in S_2 \tag{1c}$$

$$0 = \left[-K_2\bar{J}_1 - \frac{L_2}{\eta_2^2}\bar{M}_1 + (K_3+K_5)\bar{J}_3 + \left(\frac{L_3}{\eta_2^2} + \frac{L_5}{\eta_3^2}\right)\bar{M}_3 + K_4\bar{J}_5 + \frac{L_4}{\eta_2^2}\bar{M}_5\right]_{\text{tang}}, \bar{r} \in S_2 \tag{1d}$$

$$0 = \left[-L_2\bar{J}_1 + K_2\bar{M}_1 + L_3\bar{J}_3 - K_3\bar{M}_3 + (L_4+L_6)\bar{J}_5 - (K_4+K_6)\bar{M}_5\right]_{\text{tang}}, \bar{r} \in S_3 \tag{1e}$$

$$0 = \left[-K_2\bar{J}_1 + \frac{L_2}{\eta_2^2}\bar{M}_1 + K_3\bar{J}_3 + \frac{L_3}{\eta_2^2}\bar{M}_3 + (K_4+K_6)\bar{J}_5 + \left(\frac{L_4}{\eta_2^2} + \frac{L_6}{\eta_4^2}\right)\bar{M}_5\right]_{\text{tang}}, \bar{r} \in S_3 \tag{1f}$$

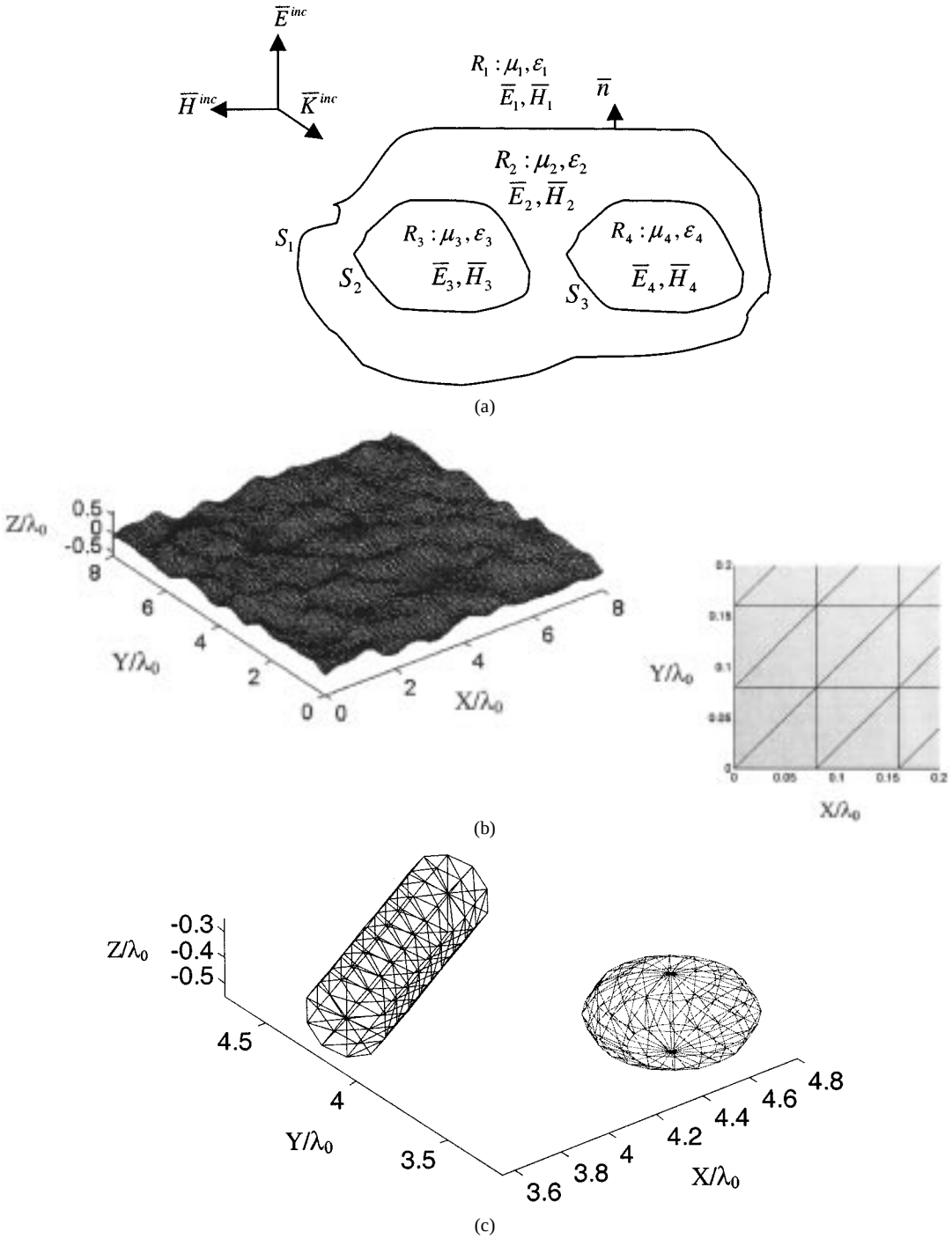

Fig. 2. (a) Two scatterers, R_3 and R_4, immersed in region R_2 immersed in region R_1 and (b) triangular mesh for the rough ground (upper figure), for the oblate spheroid and the horizontal cylinder (lower figure).

interaction scenarios; the self-interactions of the ground ($\bar{Z}_{11}$), target ($\bar{Z}_{22}$) and clutter object ($\bar{Z}_{33}$), the target with the ground and with clutter object ($\bar{Z}_{12}, \bar{Z}_{23}$) and the clutter object with the ground $\bar{Z}_{13}$, etc. The expressions of these submatrices are given in Appendix B. The tested tangential incident electric field $\bar{E}^{inc}$ and the tested normalized magnetic field $\eta_1 \bar{H}^{inc}$ on the exterior surface of the ground are expressed as part of vector $\bar{V}$ in (3) while the vector $\bar{I}$ represents the unknown current coefficients on all involved surfaces.

The emphasis of this study is to investigate the statistics of the target signature versus the clutter signature. The proposed strategy is to use the same sample of random rough surface realizations four times as follows:

i) once to compute the scattering from the rough ground alone (no buried objects);
ii) once to compute the scattering from the rough ground when both the target and clutter object are buried beneath the interface;
iii) once to compute the scattering from the rough ground when only the target is buried beneath the interface;
iv) once to compute the scattering from the rough ground when only the clutter object is buried beneath the interface.

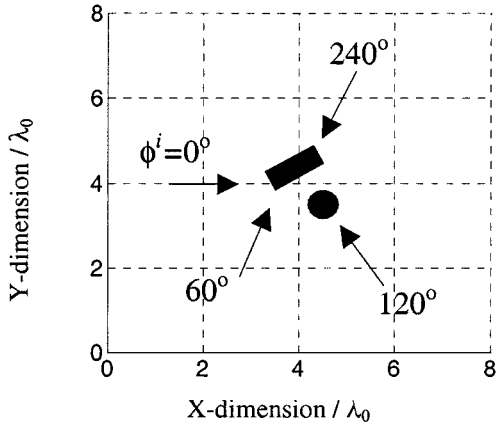

(a)

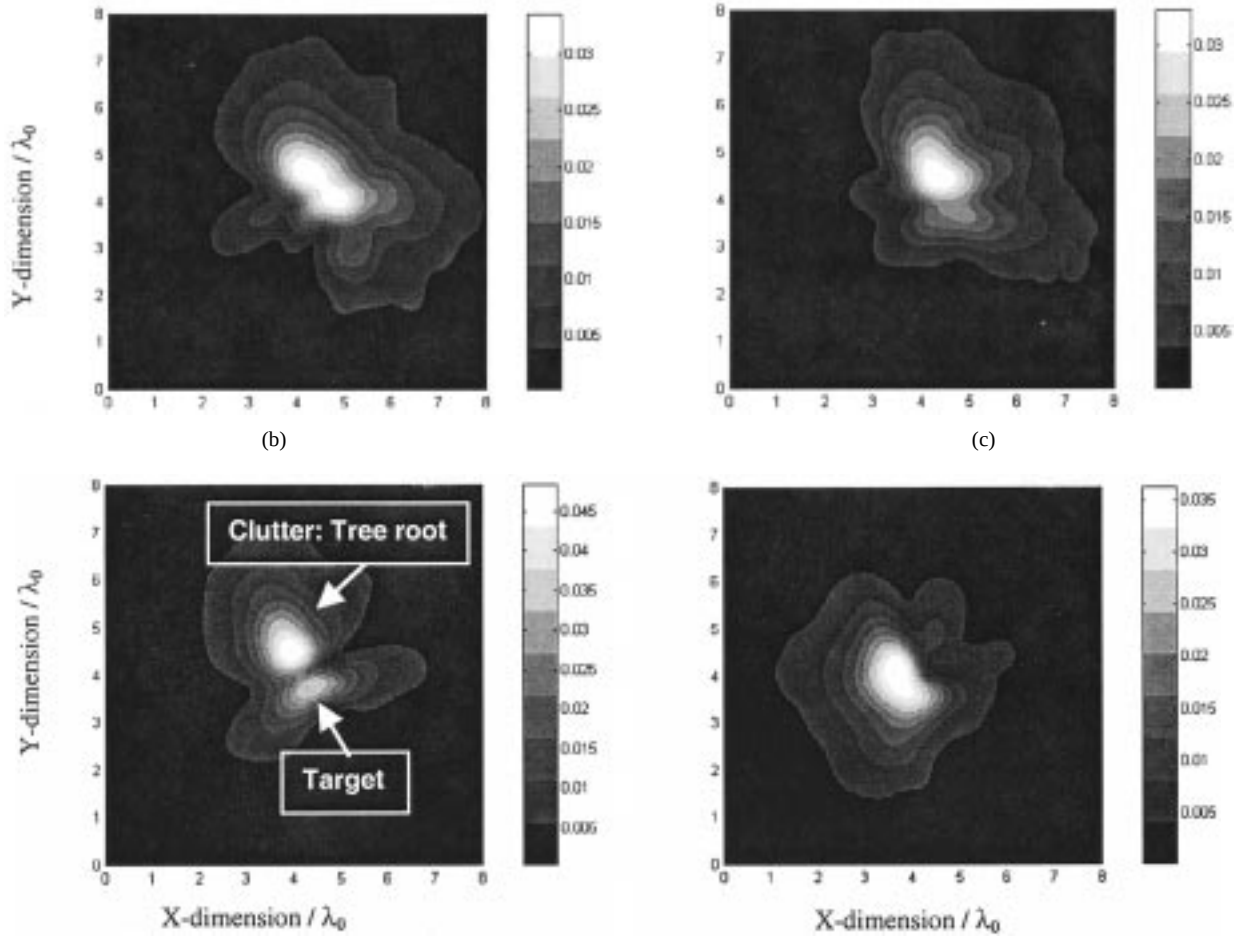

Fig. 3. (a) Top view of the target (oblate spheroid) and the tree root (horizontal cylinder), (b-e) The scattered electric field at multiple views for both the buried mine-like target and the tree root upon removing the scattering from ground when: (b) $\phi^i = 0°$, (c) $\phi^i = 60°$,(d) $\phi^i = 120°$, and (e) $\phi^i = 240°$. All results are for $\sigma = 0.1\lambda_0$, $l_c = 0.5\lambda_0$, $\theta^i = 30°$ and H-polarization.

The scattered electric near-fields are obtained in this procedure at single incident angle, single frequency, for specific polarization (e.g., vertical or horizontal), etc. This shows that conducting the Monte Carlo simulations is computationally expensive requiring fast methods such as the SDFMM. In this case, the computational complexity of the problem will be of $O(K = 2N_1 + 2N_2 + 2N_3)$ as described earlier. Once the electric and magnetic surface currents are obtained, then the scattered fields above the ground and in the near-zone can be calculated using the surface integrations given by [17]

$$\bar{E}^A(x,y,z) = -\frac{1}{4\pi(i\omega\varepsilon_0)}\nabla\times\iint_{S'}\left(\hat{R}\times\bar{J}_1(x',y',z')\right)\cdot\frac{1+ik_0R}{R^2}\exp(-ik_0R)\,dS' \quad (4a)$$

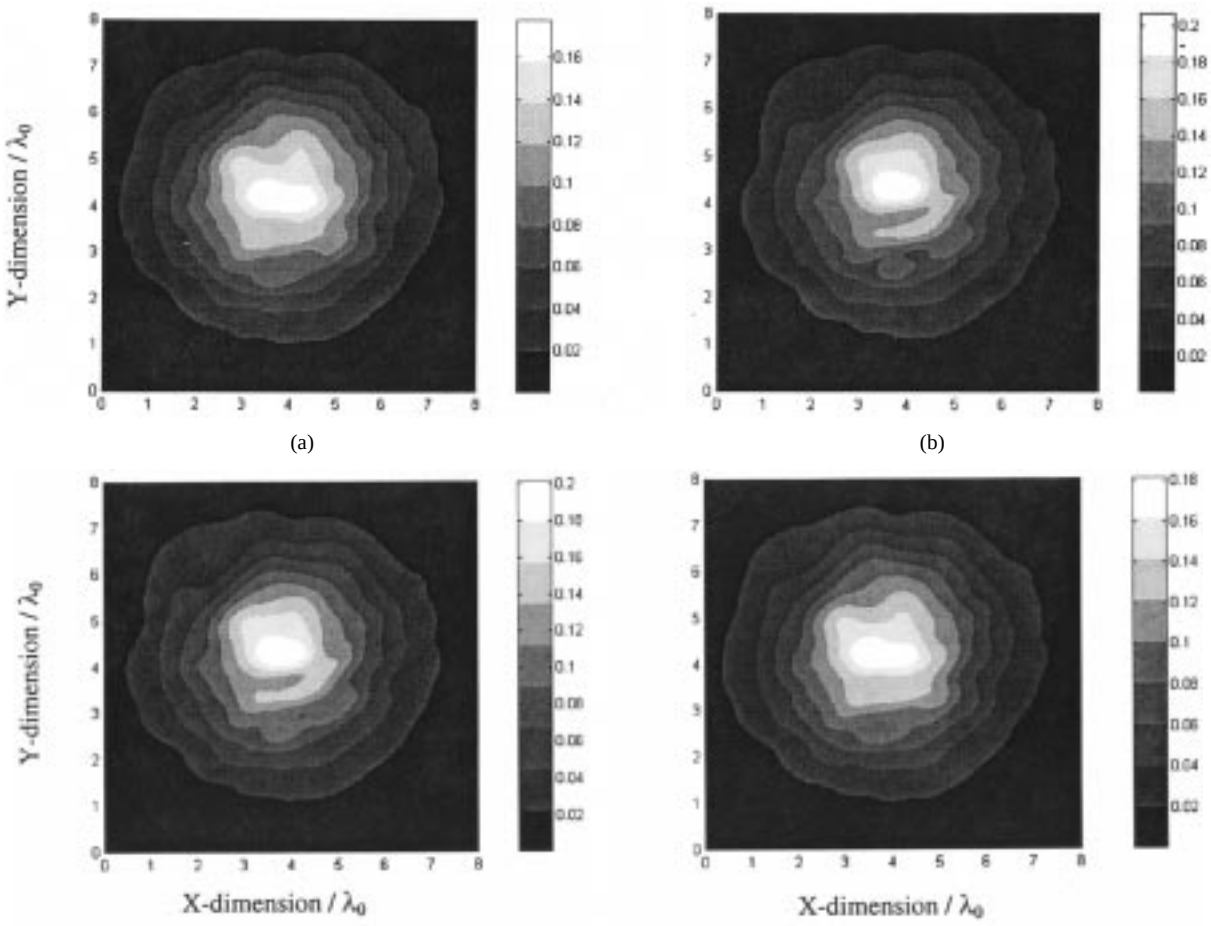

Fig. 4. Average scattered electric field at $z = 0.5\lambda_0$ from: (a) the ground with no buried objects, (b) the ground with both the buried mine-like target and tree root, (c) the ground with only the buried tree root (no mine), and (d) the ground with only the buried mine-like target (no tree root). Data are from Fig. 3(c) (H-polarization).

$$\bar{E}^F(x,y,z) = -\frac{1}{4\pi}\nabla \times \iint_{S'} \bar{M}_1(x',y',z') \cdot \frac{\exp(-ik_0R)}{R} dS' \tag{4b}$$

where the total electric field is $\bar{E}^A + \bar{E}^F$, the superscripts A and F refer to the vector potentials $\bar{A}$ and $\bar{F}$, the point source (x', y', z') is located on the ground while the observation point (x, y, z) is located above the ground, $\hat{R}$ and R are the unit vector and the distance between the observation and the source points, k_0, ε_0 and μ_0 are the wave number, the permittivity and permeability of the free space, respectively and dS' is the differential surface element on the rough ground. Every source point (x', y', z') in (4) is the centroid of every triangular patch on the ground at which the surface currents are approximately evaluated [15].

III. Numerical Results

The principle of computing the target signature at multiple views was employed in [9] and [11] by rotating the incident beam around the target, i.e., changing the azimuth angle of the incident waves. As presented in [14], when the target is buried nearby a second object, a significant electromagnetic interference between the two objects is observed in the scattered fields at single azimuth angle. In this work, the Monte Carlo simulations will be conducted using the incident beam view (azimuth angle) that largely indicates the presence of a clutter object buried nearby the target.

Trying to simulate the ground penetrating radar (GPR) of center frequency 1 GHz experiments reported in [18]–[19], the scattered electric fields at $\lambda_0/2$ above the rough ground mean are computed, where λ_0 is the free space wavelength. In addition, to simulate the GPR experimental track, the ground is modeled as a plane of dimensions $8\lambda_0 \times 8\lambda_0$. For the same reason, all simulations are conducted here at 1 GHz; however, the current technique was successfully applied for the frequency band 800 MHz–1.4 GHz (not presented here). The rough ground surface is characterized with Gaussian statistics for the heights, assuming zero mean and root mean square (rms) σ and for the autocorrelation function with correlation length l_c. It was observed that the incident beam pattern of the GPR parabolic antenna reported in [18], [19] resembles a Gaussian beam. Thus for simplicity, the incident wave in the current simulations is assumed to be a Gaussian beam tapered toward the edges of the ground with half-beam width of $1.6\lambda_0$ centered at $x = y = 4\lambda_0$[9], [20]. The incident angle of the beam, measured from the z-direction, is $\theta^i = 30^\circ$ while the

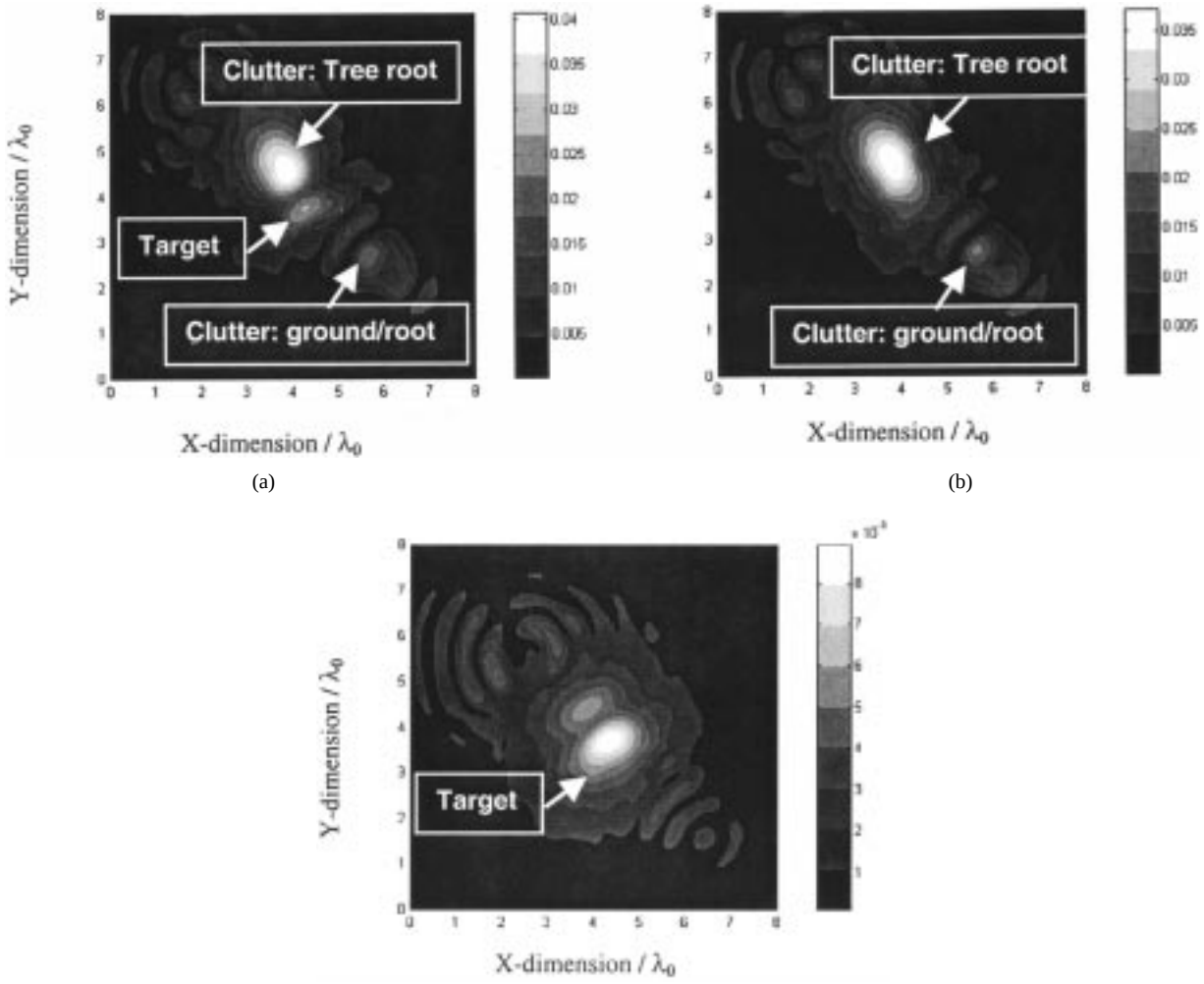

Fig. 5. Average scattered electric field upon removing the scattering from the rough ground for: (a) both the mine-like target and tree root, (b) just the tree root, and (c) just the mine-like target. Data are from Fig. 3(c) (H-polarization).

azimuth angle ϕ^i will be described. As mentioned in Section I, the AP-mine-like target is modeled here as an oblate spheroid with dimensions $a = 0.15\lambda_0$, $b = 0.3\lambda_0$ [see Fig. 2(b)] where its center is located at $x = 4.5\lambda_0$, $y = 3.5\lambda_0$ and $z = -0.4\lambda_0$ (lower right quadrant of the ground as shown in Fig. 3(a). While, the clutter object is modeled as a horizontal cylinder [see Fig. 2(b)] such as a piece of a tree root with radius $a = 0.15\lambda_0$ and height $h = 0.9\lambda_0$ with its axis tilted at angle 30° with the x-direction and located at $x = 4.01\lambda_0$, $y = 4.375\lambda_0$ and $z = -0.4\lambda_0$ measured from the axis mid-point (upper left quadrant of the ground as shown in Fig. 3(a). This implies a $1.0\lambda_0$ distance separating the centers of the two objects. In [14], a parametric study was conducted for different ground roughness in which the clutter for $\sigma = 0.1\lambda_0$ was shown, as expected, to be stronger than that of $\sigma = 0.04\lambda_0$[11]. Therefore, in this work, the rms height is assumed to be $\sigma = 0.1\lambda_0$ with correlation length $l_c = 0.5\lambda_0$. The relative dielectric constants of the soil, the AP-mine-like target and the tree root object are assumed to be $\varepsilon_r = 2.5 - j0.18$ (Bosnian soil with 3.8% moisture at 1 GHz) [21], $\varepsilon_r = 2.9 - j0.072$ (TNT) [22] and $\varepsilon_r = 4.0$ (dry wood) [23], respectively. The near-electric fields are computed using (4) at point receivers located at $z = 0.5\lambda_0$ above the ground with resolution equal to $x = y = 0.04\lambda_0$. Several numerical experiments, depending on the dielectric constants and on the ground roughness parameters, were conducted to choose the discretization distances on all surfaces. The adopted criterion is to obtain a solution that is independent of these distances. In this work, $0.08\lambda_0$ discretization distance on the rough ground is used leading to 60 000 ($2N_1$) current unknowns on its surface. For the two objects, approximately the same discretization distances are used leading to 600 ($2N_2$) on the AP-mine-like target and 600 ($2N_3$) on the tree root. The triangular mesh for the rough ground, the target (oblate spheroid) and the tree root (horizontal cylinder) is shown in Fig. 2(b). To speedup the solution's convergence, a pre-conditioner consists of the diagonal self-elements of $\bar{\bar{Z}}$ in (3) is used. A relative residual error of 10^{-3} is used in the transpose-free-quasi-minimal-residual (TFQMR) iterative solver [24] and $0.32\lambda_0 \times 0.32\lambda_0$ is assumed for the smallest fast multipole method (FMM) block size. Moreover, the SDFMM is validated with the method of moments (MoM) as discussed in [14]. The complex subtraction process is used in this work to remove the clutter due to both the random rough ground and the benign object (tree root) leading to obtain a statistical study of the target signature compared with these sources of

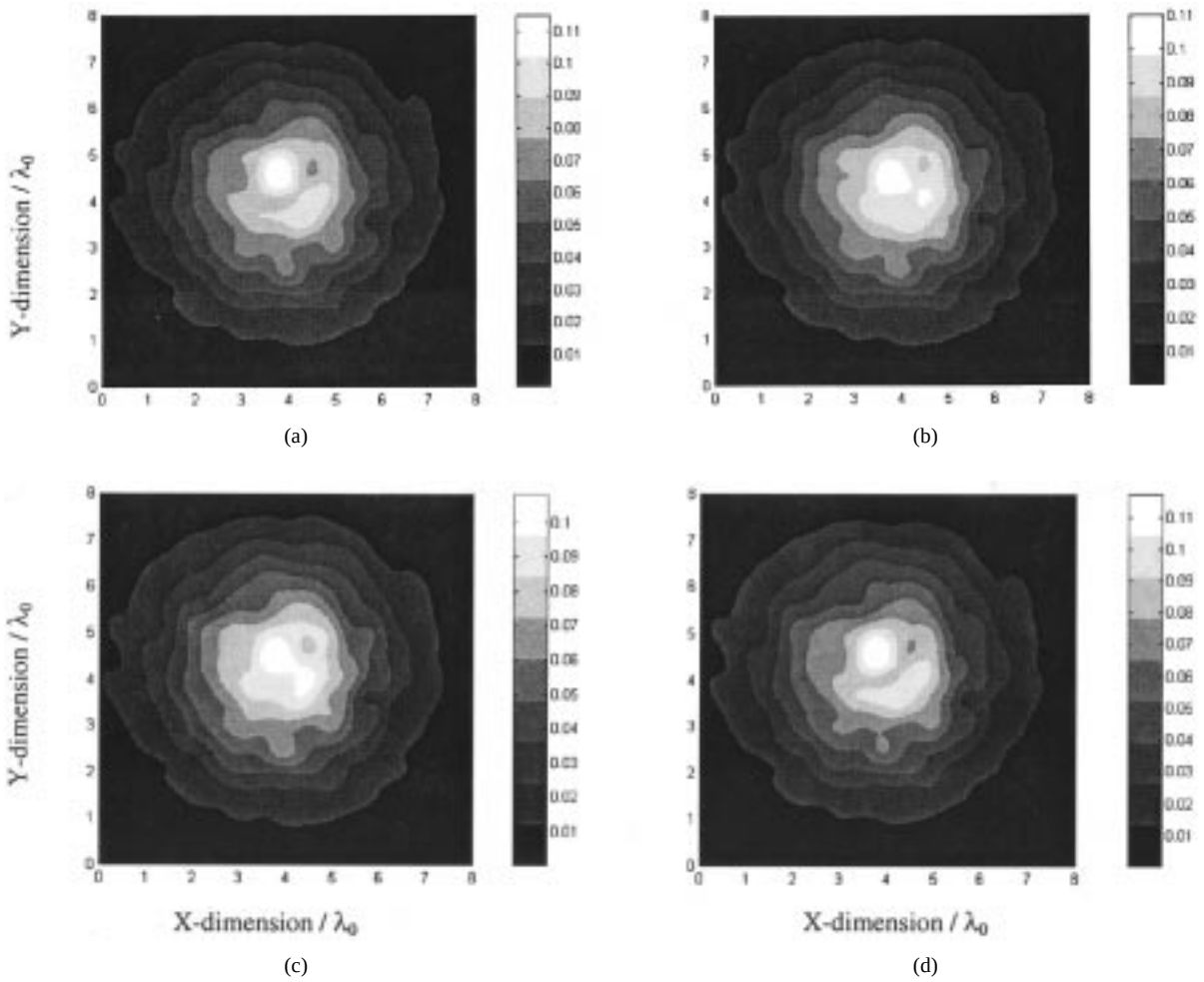

Fig. 6. Average scattered electric field at $z = 0.5\lambda_0$ from: (a) the ground with no buried objects, (b) the ground with both buried the mine-like target and tree root, (c) the ground with only the buried tree root (no mine), and (d) the ground with only the buried mine-like target (no tree root). Data are from Fig. 3(c) for V-polarization.

clutter [25]. The numerical results are divided into subsections as follows.

A. Multiple Views

The azimuth angle of the incident beam is varied as $\phi^i = 0°, 30°, 60°, \ldots, 120°$ (i.e., the azimuth angle of the plane of incidence). The fields scattered from just the rough surface realization (no buried objects) is computed and subtracted from those scattered from the same rough surface realization when both the AP-mine-like target and the tree root are buried and shown in Fig. 3(a). The results for the incident horizontal polarization are considered in this case where the electric field is perpendicular to the plane of incidence. Only four results are presented for $\phi^i = 0°, 60°, 120°$, and 240° in Fig. 3(b)–(e). The results show almost no indication to the presence of two separate objects except at $\phi^i = 120°$ where the mine-like target signature can be distinguished from that of the tree root. At this azimuth angle, the plane of incidence is perpendicular to the tree root axis. The results of Fig. 3(b)–(e) are for single rough surface realization. The interesting view at $\phi^i = 120°$ will be used in all Monte Carlo simulations considered in this work for both polarizations.

B. Monte Carlo Simulations

A sample of 100 independent random rough surface realizations was used in this work. However, the fields scattered from the geometry shown in Fig. 1 and described above was computed 800 times; 400 times for the horizontal polarization and 400 times for the vertical polarization as described in cases (i-iv) in Section II. The statistical average of the electric fields, i.e., $\langle \bar{E} \rangle$ and the standard deviation (STD), i.e., $\sqrt{\left\langle \left|\bar{E}\right|^2 \right\rangle - \left|\langle \bar{E} \rangle\right|^2}$, are presented [10]. It is necessary to mention that in the horizontal polarization case, the incident electric field is parallel to the tree root axis, while in the vertical polarization case it is perpendicular to its axis.

1) Horizontal Polarization: The results of the cases (i–iv) are plotted versus the x- and y-directions and shown in Fig. 4(a)–d, respectively. The slight differences between the results in these figures clearly indicate that the rough ground is dominating the scattering scenario. Then, the results of case i) are subtracted from those of case ii) and the output is plotted in Fig. 5(a) where the average signature of both the clutter object and the target are shown. In addition, a clutter due to the interaction between the tree root and the rough ground is clearly observed in Fig. 5(a). Similarly, the results of case iii)

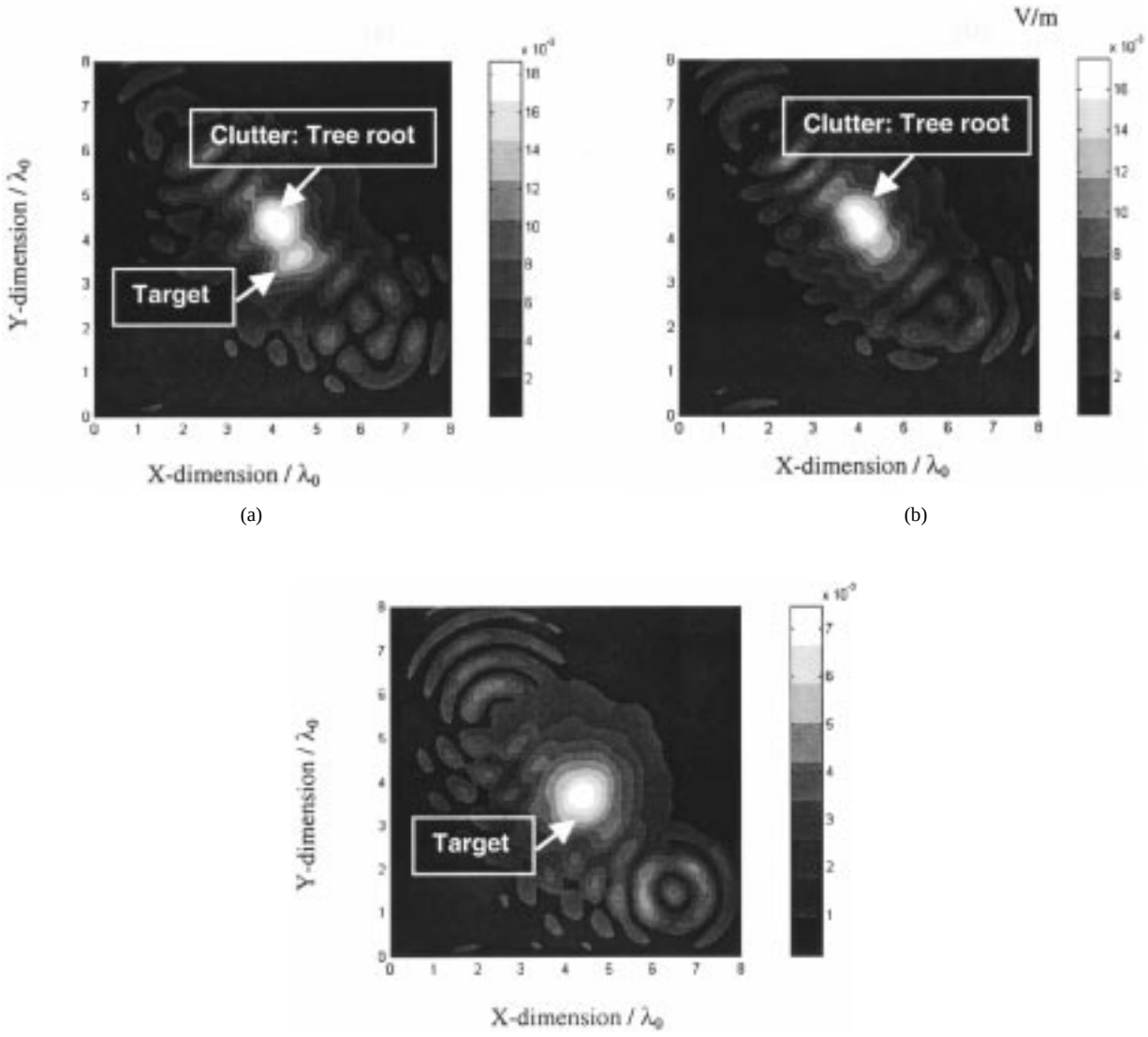

Fig. 7. Average scattered electric field upon removing the scattering from the rough ground for: (a) both the mine-like target and tree root, (b) just the tree root, and (c) just the mine-like target. Data are from Fig. 3(c) but for V-polarization.

are subtracted from those of case ii) and the output is plotted in Fig. 5(b) where the average signature of just the tree root is shown in addition to clutter due to interaction with the nearby target. Finally, the results of case iv) are subtracted from those of case ii) and the output is plotted in Fig. 5(c) where the average signature of just the target is shown in addition to interaction with the clutter object. It is important to mention that the subtraction process does not completely remove the effect of the rough ground or the nearby object; however, the remainder of these interactions depends on the ground roughness and the object proximity [14]. The results of Fig. 5(c) show a remarkable difference between the magnitude of the clutter object average signature (max. of 0.037 V/m) and that of the target average signature (max. of 0.009 V/m). Moreover in Fig. 5(a), the presence of the target causes the magnitude of the clutter object signature to slightly increase due to the interactions with the target as discussed in [14]. All these results, which are obtained using the same 100 rough surface realizations, show that a false alarm is highly possible due to the presence of a nearby clutter object (a piece of a tree root in this case).

2) Vertical Polarization: Upon changing the incident fields to the vertical polarization, then cases (i–iv) are re-computed and plotted in Fig. 6(a)–(d), respectively. In these figures, the maximum magnitude of the average scattered electric fields has dropped by almost 50%, even for the case of rough ground alone, compared with the horizontal polarization results in Fig. 5. This is because the incident electric fields at oblique angle are decomposed into two components; a component in the z-direction and a component parallel to the x–y plane (perpendicular to the tree root axis). While for the horizontally polarized incident fields, all the electric fields are parallel to the x–y plane (parallel to the tree root axis). Similarly, results of Fig. 6(a)–(d) show that the rough ground is dominating the scattering mechanism such that a slight difference between the results in Fig. 6(a)–(d) can be observed. The subtraction process is repeated in this case and the average signature of both the clutter object and the target is shown in Fig. 7(a),

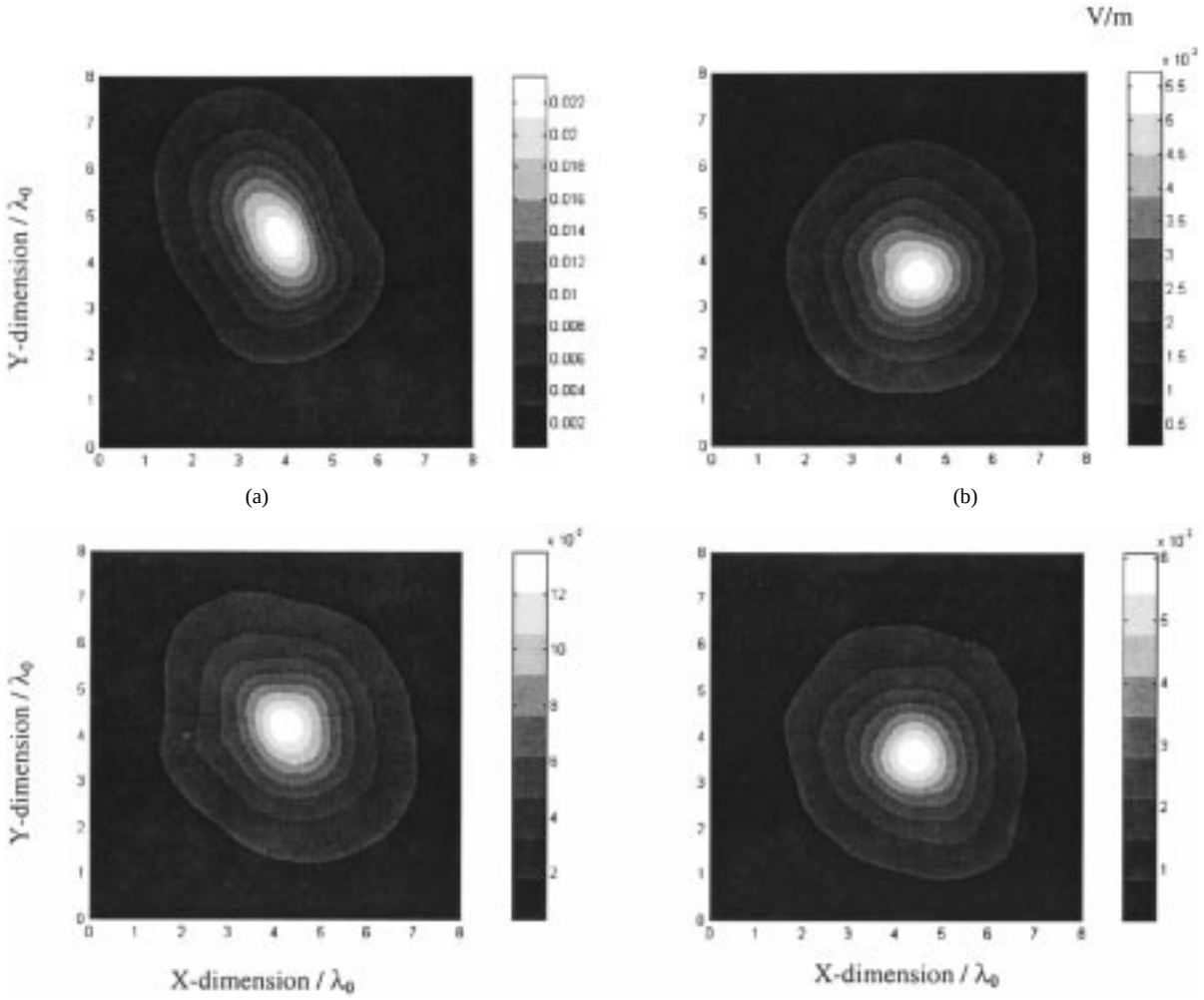

Fig. 8. Standard deviation of the scattered electric fields for (a) just the tree root, (b) just the AP-mine-like target, for the H-polarization, (c) just the tree root, and (d) jut the AP-mine-like target, for the V-polarization. Data are from Fig. 3(c).

of just the clutter object is shown in Fig. 7(b) and of just the target is shown in Fig. 7(c). The magnitude of the average target signature (max. of 0.0075 V/m) is smaller than that of the clutter object (max of 0.018 V/m), which agrees with the observation in the horizontal polarization case.

The standard deviation of the scattered fields is plotted in Fig. 8(a) for just the tree root, in Fig. 8(b) for just the target for the horizontal polarization. In theses figures, the maximum standard deviation occurs almost at the location of the tree root as shown in Fig. 8(a) and of the target as shown in Fig. 8(b). For the vertical polarization case, the standard deviation is plotted in Fig. 8(c) and (d) for the tree root and for the target, respectively. However, the results show that the maximum standard deviation of the clutter object is shifted from the location of the object. This could be attributed to the electromagnetic interference between the target and the clutter object [14]. In addition, the maximum magnitude of the standard deviation of the target signature is almost the same for both polarizations, however, for the tree root it is reduced by almost 50% in the vertical polarization. Therefore, the relative statistics are computed with respect to signature of the ground without buried objects (i.e., object signature/ground signature) as summarized in Table I.

TABLE I
MAXIMUM RELATIVE STATISTICS FOR THE SCATTERED ELECTRIC FIELDS

	Maximum relative average		Maximum relative STD	
	Clutter object	Target	Clutter object	Target
H-Pol.	20%	5%	12%	3%
V-Pol.	16%	6.5%	7.5%	3.5%

The total CPU time required for computing the scattered electric fields from one surface realization is less than 3 h (after almost 200 TFQMR iterations) and the required computer memory is 850 MB. These computations were conducted using the Compaq Alpha Server (GS140 EV6) with 667 MHz clock speed [14].

It is necessary to mention that the current work is not a signal processing technique that can be applied to the real measured data [26]. However, the current technique presents a powerful computational tool to analyze, study and statistically estimate some of the causes of false alarms encountered in the detection process.

$$\bar{Z}_{11}=\begin{pmatrix}\langle\bar{j}_1,(L_1+L_2)\,\bar{j}_1\rangle_{S_1} & \langle\bar{j}_1,-\eta_1\,(K_1+K_2)\,\bar{j}_1\rangle_{S_1}\\ \langle\bar{j}_1,\eta_1\,(K_1+K_2)\,\bar{j}_1\rangle_{S_1} & \left\langle\bar{j}_1,\eta_1^2\left(\frac{L_1}{\eta_1^2}+\frac{L_2}{\eta_2^2}\right)\bar{j}_1\right\rangle_{S_1}\end{pmatrix} \tag{B1}$$

$$\bar{Z}_{12}=\begin{pmatrix}\langle\bar{j}_1,-L_3\bar{j}_2\rangle_{S_1} & \langle\bar{j}_1,\eta_1K_3\bar{j}_2\rangle_{S_1}\\ \langle\bar{j}_1,-\eta_1K_3\bar{j}_2\rangle_{S_1} & \left\langle\bar{j}_1,-\eta_1^2\left(\frac{L_3}{\eta_2^2}\right)\bar{j}_2\right\rangle_{S_1}\end{pmatrix},$$

$$\bar{Z}_{13}=\begin{pmatrix}\langle\bar{j}_1,-L_4\bar{j}_3\rangle_{S_1} & \langle\bar{j}_1,\eta_1K_4\bar{j}_3\rangle_{S_1}\\ \langle\bar{j}_1,-\eta_1K_4\bar{j}_3\rangle_{S_1} & \left\langle\bar{j}_1,-\eta_1^2\left(\frac{L_4}{\eta_2^2}\right)\bar{j}_3\right\rangle_{S_1}\end{pmatrix} \tag{B2}$$

$$\bar{Z}_{23}=\begin{pmatrix}\langle\bar{j}_2,L_4\bar{j}_3\rangle_{S_2} & \langle\bar{j}_2,-\eta_1K_4\bar{j}_3\rangle_{S_2}\\ \langle\bar{j}_2,\eta_1K_4\bar{j}_3\rangle_{S_2} & \left\langle\bar{j}_2,\eta_1^2\frac{L_4}{\eta_2^2}\bar{j}_3\right\rangle_{S_2}\end{pmatrix} \tag{B3}$$

IV. Conclusions

The statistics of the target, the rough ground and the clutter object signatures depend on several factors such as the orientation, dielectric constants, proximity between objects, burial depth, etc. For the parameters used in this work, the statistical study showed that the target signature appears much weaker than the clutter object signature even for a small realistic nearby buried object such as a piece of a tree root. Moreover, consistent with our previous work [10]–[11], the rough ground clutter dominates the scattering scenario necessitating its removal in the detection process. The conducted statistical study is based on running the 3-D scattering computer code more than 800 times which could not be achieved without using a fast algorithm such as the SDFMM.

Appendix A

With representing the surface electric and magnetic currents $\bar{J}$ and $\bar{M}$ on S_1, S_2 and S_3 by the vector $\bar{X}$, the integro-differential operators L_j and K_j, $j=1,2,\ldots 6$, are [14], [16]:

$$\begin{aligned}L_{1,2}\bar{X}&=\int_{S_1}\left\{i\omega\mu_{1,2}\Phi_{1,2}\bar{X}\,(\bar{r}')\right.\\&\qquad\left.+\frac{i}{\omega\varepsilon_{1,2}}\nabla\nabla'\cdot\bar{X}\,(\bar{r}')\,\Phi_{1,2}\right\}ds',\\K_{1,2}\bar{X}&=\int_{S_1}\bar{X}\,(\bar{r}')\times\nabla\Phi_{1,2}ds'\end{aligned} \tag{A1}$$

$$\begin{aligned}L_{3,5}\bar{X}&=\int_{S_2}\left\{i\omega\mu_{2,3}\Phi_{2,3}\bar{X}\,(\bar{r}')\right.\\&\qquad\left.+\frac{i}{\omega\varepsilon_{2,3}}\nabla\nabla'\cdot\bar{X}\,(\bar{r}')\,\Phi_{2,3}\right\}ds',\\K_{3,5}\bar{X}&=\int_{S_2}\bar{X}\,(\bar{r}')\times\nabla\Phi_{2,3}ds'\end{aligned} \tag{A2}$$

$$\begin{aligned}L_{4,6}\bar{X}&=\int_{S_3}\left\{i\omega\mu_{2,4}\Phi_{2,4}\bar{X}\,(\bar{r}')\right.\\&\qquad\left.+\frac{i}{\omega\varepsilon_{2,4}}\nabla\nabla'\cdot\bar{X}\,(\bar{r}')\,\Phi_{2,4}\right\}ds',\\K_{4,6}\bar{X}&=\int_{S_3}\bar{X}\,(\bar{r}')\times\nabla\Phi_{2,4}ds'\end{aligned} \tag{A3}$$

Appendix B

The elements of the submatrix $\bar{Z}_{11}$ in (3) are given by [14], [16] (B1), shown at the top of the page, in which $\langle\bar{A},\bar{B}\rangle_S$ denotes the complex inner product between vector functions $\bar{A}$ and $\bar{B}$ on a surface S. The submatrices $\bar{Z}_{12}$, $\bar{Z}_{13}$, and $\bar{Z}_{23}$ are given by (B2)–(B3), shown at the top of the page. Similar expressions can be obtained for all other submatrices in (3).

Acknowledgment

The authors would like to thank V. Jandhyala, E. Michielssen, and W. Chew, UIUC, for the original development of the SDFMM.

References

[1] P. Beckmann and A. Spizzichino, *The Scattering of Electromagnetic Waves From Rough Surfaces.* New York: Macmillan, 1963.

[2] E. Bahar and M. El-Shenawee, "Double scatter cross sections for two dimensional random rough surfaces that exhibit backscatter enhancement," *J. Opt. Soc. Amer. A*, vol. 18, no. 1, pp. 108–116, Jan. 2001.

[3] A. Ishimaru and J. S. Chen, "Scattering from very rough metallic and dielectric surfaces: A theory based on the modified Kirchhoff approximation," *Waves Random Media*, pp. 21–34, Jan. 1991.

[4] E. Thorsos, "The validity of the Kirchhoff approximation for rough surface scattering using a Gaussian roughness spectrum," *J. Acoust. Soc. Amer.*, vol. 83, no. 1, 1988.

[5] R. L. Wagner, J. Song, and W. C. Chew, "Monte Carlo simulation of electromagnetic scattering from two-dimensional random rough surfaces," *IEEE Trans. Antennas Propagat.*, vol. 45, pp. 235–245, Feb. 1997.

[6] V. Jandhyala, E. Michielssen, B. Shanker, and W. C. Chew, "A combined steepest descent-fast multipole algorithm for the fast analysis of three-dimensional scattering by rough surfaces," *IEEE Trans. Geosci. Remote Sensing*, vol. 36, pp. 738–748, May 1998.

[7] J. T. Johnson, L. Tsang, R. T. Shin, K. Pak, C. H. Chan, A. Ishimaru, and Y. Kuga, "Backscattering enhancement of electromagnetic waves from two-dimensional perfectly conducting random rough surfaces: A comparison of Monte Carlo simulations with experimental data," *IEEE Trans. Antennas Propagat.*, vol. 44, pp. 748–756, May 1996.

[8] L. Tsang, C. H. Chan, K. Pak, H. Sangani, A. Ishimaru, and P. Phu, "Monte Carlo simulations of large-scale composite random rough-surface scattering based on the banded-matrix iterative approach," *J. Opt. Soc. Amer.*, vol. 11, no. 2, pp. 691–696, 1994.

[9] G. Zhang, L. Tsang, and K. Pak, "Angular correlation function and scattering coefficient of electromagnetic waves scattered by a buried object under a two-dimensional rough surface," *J. Opt. Soc. Amer. A*, vol. 15, no. 12, pp. 2995–3002, Dec. 1998.

[10] M. El-Shenawee, C. Rappaport, and M. Silevitch, "Monte Carlo simulations of electromagnetic wave scattering from random rough surface with 3-D penetrable buried object: Mine detection application using the SDFMM," *J. Opt. Soc. Amer. A*, Dec. 2001.
[11] M. El-Shenawee, C. Rappaport, E. Miller, and M. Silevitch, "3-D subsurface analysis of electromagnetic scattering from penetrable/PEC objects buried under rough surfaces: Use of the steepest descent fast multipole method (SDFMM)," *IEEE Trans. Geosci. Remote Sensing*, vol. 39, pp. 1174–1182, June 2001.
[12] V. Jandhyala, "Fast multilevel algorithms for the efficient electromagnetic analysis of quasi-planar structures," Ph.D. dissertation, Dept. Elect. Comput. Eng., Univ. Illinois, Urbana-Champaign, 1998.
[13] M. El-Shenawee and C. Rappaport, "Modeling clutter from Bosnian and Puerto Rican rough ground surfaces for GPR subsurface sensing applications using the SDFMM technique," *J. Subsurf. Sensing Technol. Applicat.*, vol. 2, pp. 249–264, July 2001.
[14] M. El-Shenawee, "Scattering from multiple objects buried under two-dimensional randomly rough surface using the steepest descent fast multipole method," *IEEE Trans. Antennas Propagat.*, to be published.
[15] S. M. Rao, D. R. Wilton, and A. W. Glisson, "Electromagnetic scattering by surfaces of arbitrary shape," *IEEE Trans. Antennas. Propagat.*, vol. AP-30, pp. 409–418, May 1982.
[16] L. Medgyesi-Mitschang, J. Putnam, and M. Gedera, "Generalized method of moments for three-dimensional penetrable scatterers," *J. Opt. Soc. Amer. A*, vol. 11, no. 4, pp. 1383–1398, April 1994.
[17] C. A. Balanis, *Advanced Engineering Electromagnetics*. New York: Wiley, 1989, ch. 6, pp. 254–309.
[18] C. Rappaport, S. Azevedo, T. Rosenbury, J. Gough, and A. Dean, "Detecting antipersonnel mines with a handheld parabolic reflector transmitter/multistatic receiver impulse GPR," in *Proc. 2000 UXO/Countermine Forum*, May 2000.
[19] C. Rappaport, S. Azevedo, T. Rosenbury, and J. Gough, "Handheld forward-looking focused array mine detection with plane wave excitation," *Proc. SPIE*, pp. 1118–1126, Apr. 2000.
[20] P. Tran and A. A. Maradudin, "Scattering of a scalar beam from a two-dimensional randomly rough hard wall: Enhanced backscatter," *Phy. Rev. B*, vol. 45, no. 7, pp. 3936–3939, Feb. 1992.
[21] J. Curtis, "Dielectric properties of soils; various sites in Bosnia," in *Station Data Report: U.S. Army Corp. of Engineers, Waterways Experiment*. Washington, DC: U.S. Army, 1996.
[22] V. Hippel, *Dielectric Materials and Applications*. New York: Wiley, 1953, p. 315.
[23] F. T. Ulaby, *Fundamentals of Applied Electromagnetics*. Englewood Cliffs, NJ: Prentice-Hall, 2001.
[24] R. W. Freund, "A transpose-free quasiminimal residual algorithm for nonhermitian linear systems," *SIAM J. Sci. Comput.*, vol. 14, no. 2, pp. 470–482, Mar. 1993.
[25] A. L. Warrick, S. G. Azevedo, and J. E. MST, "Prediction of buried mine-like target radar signature using wideband electromagnetic modeling," *Proc. SPIE*, vol. 3392, pp. 776–783, 1998.
[26] A. van der Merwe and I. J. Gupta, "A novel signal processing technique for clutter reduction in GPR measurements of small, shallow land mines," *IEEE Trans. Geosci. Remote Sensing*, vol. 38, pp. 2627–2637, Nov. 2000.

Magda El-Shenawee (M'91) received the B.S. and M.S. degrees in electrical engineering from Assiut University, Assiut, Egypt, and the Ph.D. degree in electrical engineering from the University of Nebraska, Lincoln, in 1991.

In 1992, she worked as a Research Associate in the Center for Electrooptics, University of Nebraska, where she focused on the problem of enhanced backscatter phenomena. In 1994, she was a Research Associate at the National Research Center, Cairo, Egypt, and in 1997, she was a Visiting Scholar at the University of Illinois, Urbana-Champaign. In 1999, she joined the Multidisciplinary University Research Initiative (MURI) Team, Northeastern University, Boston, MA. Currently, she is an Assistant Professor in the Department of Electrical Engineering, University of Arkansas, Fayetteville. Her research areas are rough surface scattering, computational electromagnetics, subsurface sensing of buried objects, breast cancer modeling, numerical methods, and micro-strip circuits.

Dr. El-Shenawee is a member of Eta Kappa Nu.

Carey M. Rappaport (SM'96) received the S.B. degree in mathematics, the S.B., S.M., and E.E. degrees in electrical engineering, and the Ph.D. in electrical engineering, all from the Massachusetts Institute of Technology (MIT), Cambridge, in 1982 and 1987, respectively.

He has worked as a Teaching and Research Assistant at MIT, from 1981 until 1987, and during the summers at COMSAT Labs, Clarksburg, MD, and The Aerospace Corporation, El Segundo, CA. He joined the faculty at Northeastern University, Boston, MA, in 1987. He has been Professor of electrical and computer engineering since July 2000. During Fall 1995, he was Visiting Professor of electrical engineering at the Electromagnetics Institute, Technical University of Denmark, Lyngby, as part of the W. Fulbright International Scholar Program. He has consulted for Geo-Centers, Inc., PPG, Inc., and several municipalities on wave propagation and modeling and microwave heating and safety. He is Principal Investigator of the ARO Multidisciplinary University Research Initiative in Humanitarian Demining and Co-Principal Investigator of the Center for Subsurface Sensing and Imaging Systems (CenSSIS) Engineering Research Center. He has authored over 180 technical journal and conference papers in the areas of microwave antenna design, electromagnetic scattering computation, and bioelectromagnetics, and has received two reflector antenna patents, two biomedical device patents, and three subsurface sensing device patents.

Dr. Rappaport received the IEEE Antenna and Propagation Society's H.A. Wheeler Award for best applications paper of 1985. He is a member of Sigma Xi and Eta Kappa Nu.